Applied Physics Letters

RESEARCH ARTICLE | DECEMBER 01 2025

Effects of lamella preparation on InGaN quantum well luminescence

Nika van Nielen ; Luiz H. G. Tizei ; Delphine Lagarde ; Cleo Santini ; Florian Castioni ; Robin Cours; Andrea Balocchi ; Teresa Hungria ; Andrew F. Tsatsulnikov ; Alexei V. Sakharov ; Andrew E. Nikolaev ; Nikolay Cherkashin ; Albert Polman ; Sophie Meuret

Appl. Phys. Lett. 127, 222101 (2025)
https://doi.org/10.1063/5.0283025

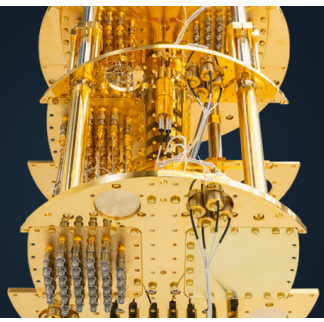

Applied Physics Letters ARTICLE pubs.aip.org/aip/apl

Effects of lamella preparation on InGaN quantum well luminescence

Cite as: Appl. Phys. Lett. **127**, 222101 (2025); doi: 10.1063/5.0283025
Submitted: 29 May 2025 · Accepted: 8 November 2025 ·
Published Online: 1 December 2025

View Online Export Citation CrossMark

Nika van Nielen,[1,a)] Luiz H. G. Tizei,[2] Delphine Lagarde,[3] Cleo Santini,[4] Florian Castioni,[2] Robin Cours,[4] Andrea Balocchi,[3] Teresa Hungria,[5] Andrew F. Tsatsulnikov,[6] Alexei V. Sakharov,[6] Andrew E. Nikolaev,[6] Nikolay Cherkashin,[4] Albert Polman,[1] and Sophie Meuret[4]

AFFILIATIONS

[1]NWO-Institute AMOLF, Amsterdam, The Netherlands
[2]Université Paris-Saclay, CNRS, Laboratoire de Physique des Solides, Orsay, France
[3]CNRS, LPCNO, Toulouse, France
[4]CEMES/CNRS, Toulouse, France
[5]CNRS, Centre de Microcaracterisation Raimond Castaing, Toulouse, France
[6]Ioffe Institute, Saint-Petersburg, Russia

Note: This paper is part of the Special Topic on Frontiers in Nitride Semiconductors Research.
[a)]**Author to whom correspondence should be addressed:** vnielen@amolf.nl

ABSTRACT

Despite it being a popular sample preparation technique, the optoelectronic effects of thinning bulk samples into lamella using a Ga-based focused ion beam (FIB), as is commonly performed for studies in a transmission electron microscope, have been seldom studied systematically. In this work, we confront this using correlative cathodoluminescence spectroscopy to investigate the optical properties of high In content c-plane InGaN/GaN quantum wells (QWs), fabricated including a growth-interrupting step that forms regions of quantum disk InGaN islands that behave as localized emitters and, furthermore, reduce the strain-induced quantum Stark effect present in the majority of such heterostructures. Using picosecond electrostatically beam-blanked electron pulses, we measured the decay transients as a function of position and wavelength. The sample was studied before and after undergoing preparation as a lamella, demonstrating that FIB preparation affects both the spectral and temporal luminescence properties despite measures undertaken to protect the sample during fabrication. Non-radiative defects introduced by the ion beam quenched the luminescence as well as reduced the lifetime of emission, with the QW luminescence component particularly affected due to the emission being weakly localized and hence allowing carriers to migrate to defect areas. These findings underscore the importance of correlating bulk and lamella properties to accurately interpret optical measurements.

Lamella preparation using focused ion beam (FIB) milling is a powerful technique in materials science, enabling the fabrication of electron-transparent and site-specific samples for atomic-scale analysis within a transmission electron microscope (TEM). This method has been applied to understand the structural and chemical features of a variety of material systems. Due to its nanoscale spatial resolution and keV energy regime, cathodoluminescence (CL) has emerged as an ideal tool for optical characterization of wide bandgap materials, such as GaN, far beyond the optical diffraction limit.[1–3] Such measurements are routinely performed in TEMs on GaN devices,[4–8] as well as other materials.[9,10] These CL-TEM studies enable the correlation of radiative properties and defect-related emission with the structure of the material at the nanoscale.

However, it is well-known that the FIB can also introduce artifacts. The ion beam has been shown to cause localized damage such as ion implantation, sputtering, amorphization, point defect creation, including vacancies, and damage from thermal effects. As these artifacts are linked to the interaction volume of the ion beam within the material, the FIB leaves a damaged layer of several tens of nm thick,[11] depending on the energy of the ion beam.[12] Hence, a large body of work has been performed to mitigate these issues and optimize the FIB parameter space.[13] This includes reduction of ion beam energy,[14] thereby reducing the collision cascade, the deposition of platinum or tungsten protective layers, utilization of chemically inert plasma beams such as Xe,[15] and post-thinning annealing to restore the crystal structure.[16]

Nonetheless, some studies are emerging indicating that despite the measures undertaken to mitigate ion-induced damage, FIB lamellae often do not replicate the radiative emission characteristics of their bulk counterparts.[17,18] These differences cannot be attributed solely to the reduction of the material dimensions via thinning (possibly modifying strain). While the implications of this research are crucial for TEM-based CL studies, where conclusions about the bulk material may be deduced from optical measurements on lamella, correlative measurements on the same material in both configurations are yet to be demonstrated.

In this work, we use scanning electron microscope (SEM)-CL to investigate the optical properties of the same region of an InGaN/GaN quantum well (QW) heterostructure in both its bulk form and as an FIB-prepared lamella. The heterostructure in our case study is composed of single quantum well (QW) and quantum disk (QD) active regions, resulting in a significant spectral variation of the CL signal with position across the sample and enabling the identification of the same region at the nanoscale before and after lamella preparation. By employing hyperspectral CL, we capture the spatially resolved emission spectra to evaluate changes in radiative spectral properties, while time-resolved CL (TR-CL) provides insight into recombination dynamics. We find that FIB preparation affects both these properties, emphasizing the need to understand its impact to be able to retrieve the bulk properties from the TEM-CL study.

The sample was grown, as demonstrated graphically in Fig. 1(a), by metalorganic vapor phase epitaxy (MOVPE) on a (001) sapphire substrate using a custom Dragon family horizontal-flow episystem with an inductively heated susceptor and standard precursors.[19] Growth started from a low-temperature GaN nucleation layer followed by thick high-temperature GaN growth to reduce dislocation density. Subsequently, the temperature was lowered, and a 4 nm layer of $In_xGa_{1-x}N$, where $x = 25\%–30\%$, was deposited in a hydrogen-free ambient. Prior to overgrowth with GaN, the InGaN was subjected to a growth-interruption (GI) step using exposure to a hydrogen-containing atmosphere. The stoichiometry of the sample was calculated using strain-state analysis (S1) of $(1\bar{1}00)$ cross-sectional high-angle annular

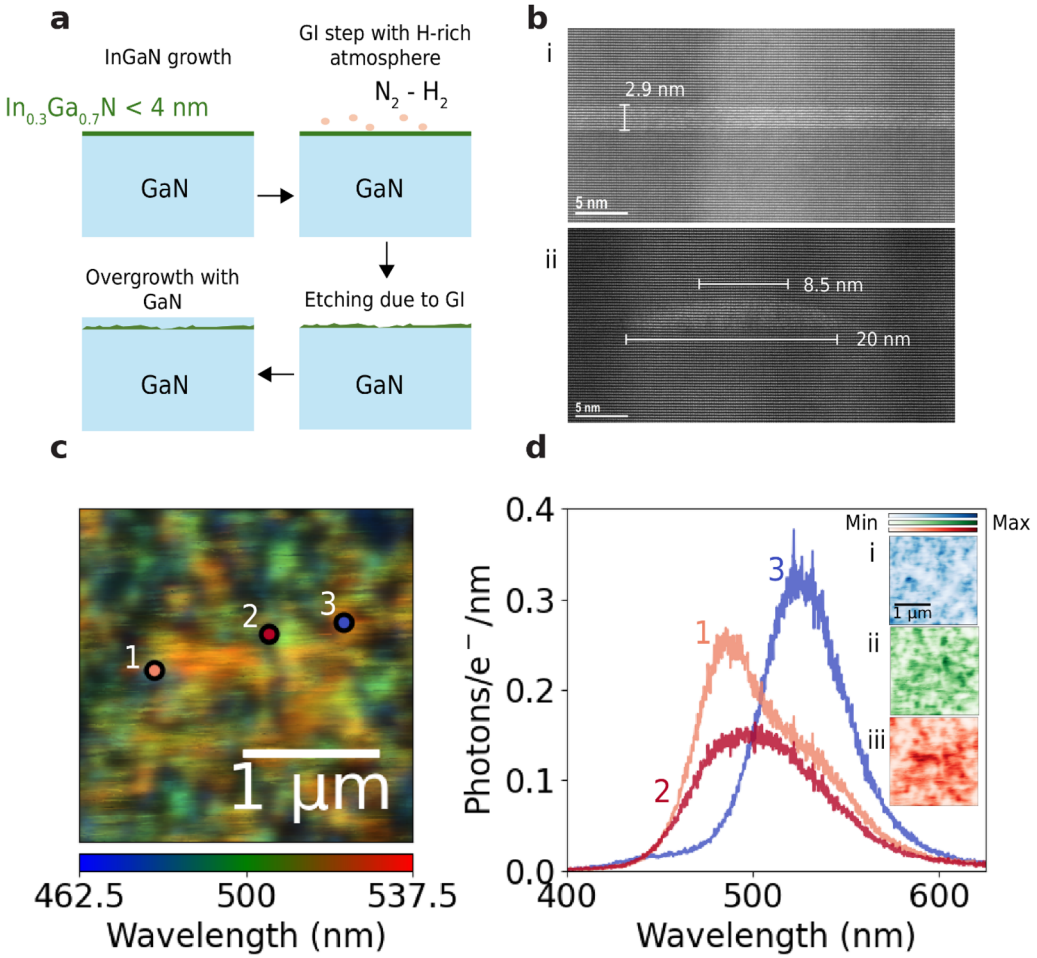

FIG. 1. (a) Graphic demonstrating InGaN/GaN QW/QD fabrication. (b) High-resolution 200 keV HAADF-STEM depicting QW (top) and QD (bottom) regions of the sample. (c) RGB SEM-CL map with pixel size 10 nm at $\lambda_c = 500 \pm 37.5$ nm of bulk sample. (d) CL spectra corresponding with measurement areas marked in (c). The insets show CL maps centered at λ_c =(i) 475, (ii) 500, and (iii) 525 nm, and bandwidth 25 nm.

dark-field scanning transmission electron microscopy (HAADF-STEM) images, which were corrected for distortion and calibration errors by applying the AbStrain procedure.[20–22] As a result of the GI step, the InGaN layer is etched, transforming the homogenous layer into areas of 2D InGaN QWs, as shown in the HAADF-STEM image in Fig. 1(bi), and 3D InGaN QDs with a lateral confinement on the order of tens of nm, Fig. 1(bii). Although this is larger than the Bohr radius in InGaN (which, depending on the stoichiometry, is between approximately 3 nm for GaN[23] and 8 nm for InN[24]), InGaN QDs of similar length scales have demonstrated blue shifting due to lateral confinement.[25,26] This fabrication approach was originally developed to promote confinement of carriers within QD regions of the sample, mitigating carriers from migrating in the QW plane to defects and dislocations,[27] and ensuring a higher EQE of resulting devices;[19] however, it additionally prevents indium phase segregation[28] and reduces the strain-induced quantum confined stark effect (QCSE) present in the majority of such structures (as evidenced in data further in the manuscript).

After full optical characterization of two identified areas on the bulk sample, we extracted two lamellae from these areas: one in cross section and another in plan view. These preparations were carried out using a gallium ion source on a ThermoFisher Helios Nanolab 600i dual-beam FIB/SEM microscope at 2×10^{-6} mbar. To protect the surface, two layers of carbon and platinum (a few hundred nanometers thick) were deposited by focused electron beam induced deposition, followed by a $\sim 1\ \mu$m layer of platinum deposited by focused ion beam induced deposition. The thick lamellae were then cut and extracted using a micromanipulator (Omniprobe 200) and mounted on a TEM grid. Final thinning to a thickness of around 200 nm was performed using a graded voltage procedure to reduce the damage caused by the FIB. The Ga beam acceleration was sequentially reduced: initially at 30 keV and 430 pA at a $+1°$ angle, followed by 16 keV at 50 pA ($+2°$), 8 keV at 20 pA ($+3°$), 5 keV at 15 pA ($+3°$), and finally 2 keV at 20 pA ($+4°$). Each milling step was monitored live using SEM imaging and was stopped once the lamella reached the desired thickness and several tens of nm of material were removed. For the lamellae in plan view, the protective layers previously deposited on the surface were milled using the FIB.

A $2 \times 2\ \mu m^2$ region of the bulk sample was characterized using cathodoluminescence experiments performed within an SEM equipped with a parabolic mirror for high-NA light collection and redirection to an optical spectrometer (see the supplementary methods). The SEM was operated at 5 keV to minimize the penetration depth and size of the electron cascade within the sample, thereby achieving a higher spatial resolution (see S2 for CASINO Monte Carlo simulations[29]). The electron beam current was set to 10 pA to mitigate damage by the electron beam.

Figure 1(c) shows the measured CL map centered at $\lambda_c = 500 \pm 37.5$ nm, fitted to false-color RGB values by splitting the wavelength range into three 25 nm channels. The spectra in Fig. 1(d) corresponding to the highlighted pixels in the RGB consistently form two discrete bands, resulting from quantum confinement effects in the inhomogeneous InGaN layer. For $\lambda_c < 500$ nm, we observe spatially localized emission [blue region in Fig. 1(di)] that we associate with the QDs. Despite their physical size, the emission from the QDs is localized to emission spots of around a hundred nanometer diameter, limited by the electron cascade and charge carrier diffusion (S2). For $\lambda_c > 500$ nm, the broader, less localized features [green and red colors in Figs. 1(dii) and 1(diii)] are associated with the QW emission.

The strong localization of the $\lambda_c < 500$ nm band is more clearly observable in STEM-CL measurements on a cross-sectional lamella from the same sample growth (Fig. 2) performed in a dedicated STEM Nion at 60 keV and liquid nitrogen temperatures, which achieves higher spatial resolution than SEM-CL. The position-dependent CL spectra in Fig. 2(a) feature the same two bands observed in SEM-CL, and the CL maps filtered for $\lambda_c = 425 \pm 5$ nm and (d) $\lambda_c = 500 \pm 50$ nm in Figs. 2(c) and 2(d) clearly show the spatial separation of the two bands. Furthermore, the lack of band-bending related red-shifting under electron beam excitation away from the QW,[30,31] resulting in a lower excitation density, suggests that the QCSE is minimal and that any internal electric fields are largely unscreened and do not dominate the recombination dynamics. More hyperspectral measurements at room temperature and time-resolved TEM-CL for direct comparison to subsequent SEM-CL results are available in S3.

Next, we repeat the SEM-based hyperspectral CL experiments on the lamella sample; the SEM was now operated at 30 keV to achieve the highest spatial resolution, and a current of 10 pA was maintained. A representative false-color RGB CL map is shown in Fig. 3(b) with corresponding spectra in Fig. 3(c). These measurements show that the InGaN layer remains luminescent after lamella preparation; however, the integrated count rate is significantly reduced. This is an anticipated feature considering that the energy deposited per electron changes by an order of magnitude as most electrons are being completely transmitted through the sample (S2). However, the counts still drop by an additional five orders of magnitude, indicating that quenching due to defect creation has occurred, primarily affecting the QW emission.

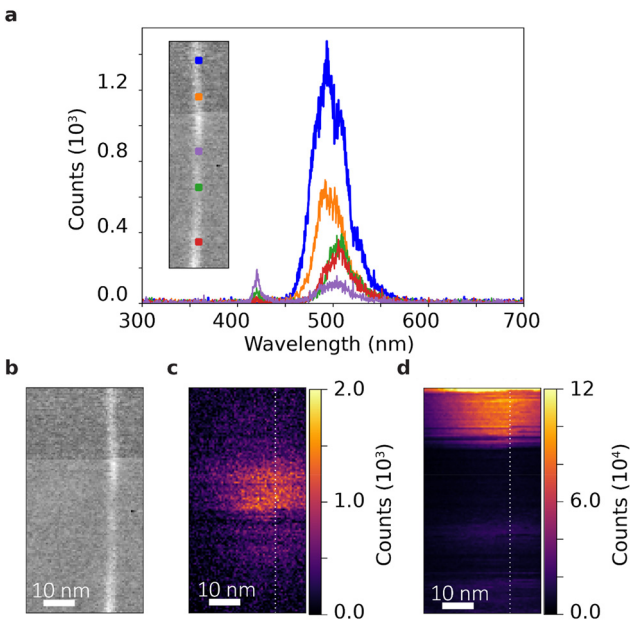

FIG. 2. Hyperspectral TEM-CL measurements on cross-sectional lamella at 60 keV. (a) CL spectra from different positions along the InGaN layer, as seen in the dark-field TEM image in (b), with CL measurement positions marked in the inset. CL maps of pixel size 0.6 nm at (c) $\lambda_c = 425 \pm 5$ nm and (d) $\lambda_c = 500 \pm 50$ nm. The dotted lines indicate the position of the InGaN layer.

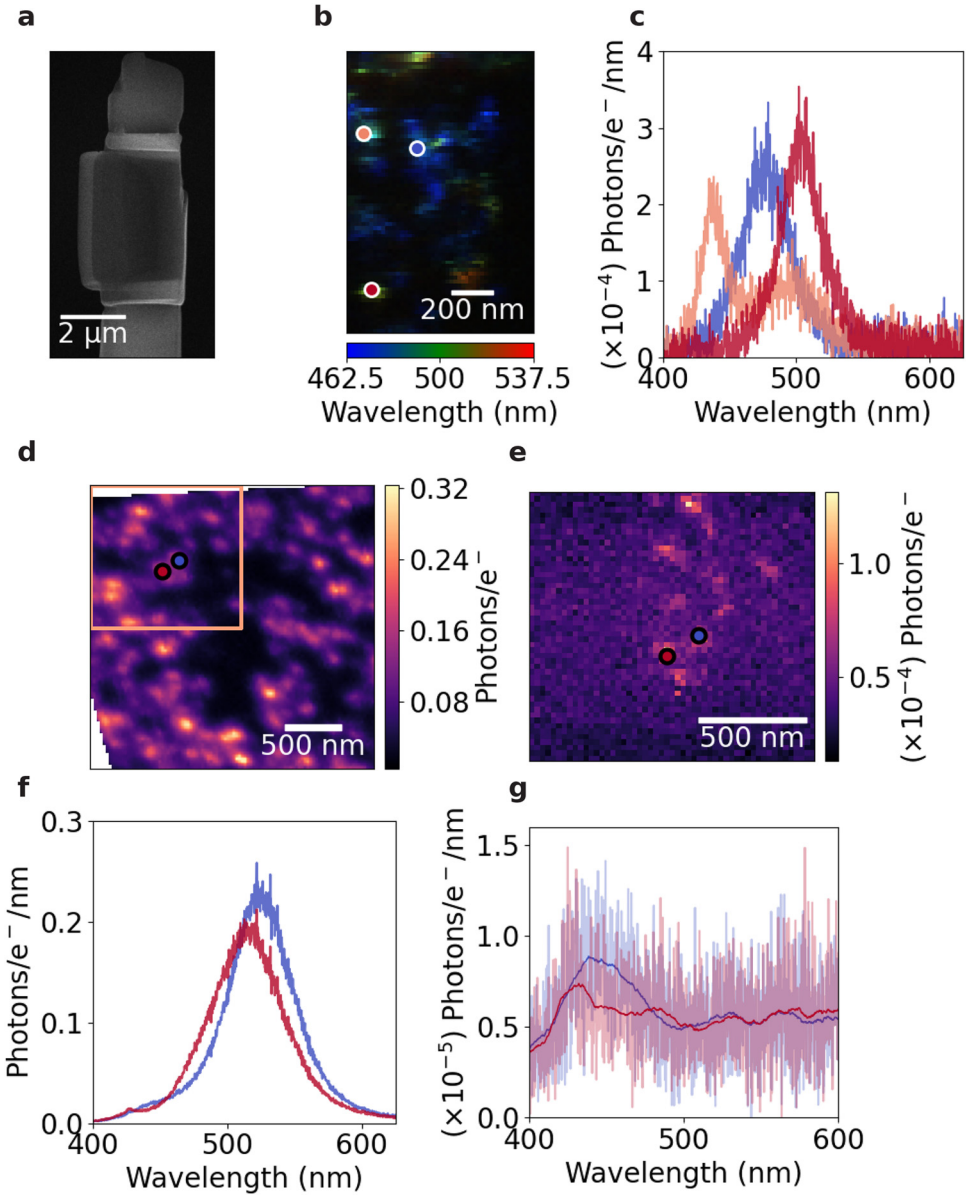

FIG. 3. (a) SEM image of the plan view lamella sample. (b) False-color RGB SEM-CL map with $\lambda_c = 500 \pm 37.5$ nm, with spectra corresponding to marked positions plotted in (c). (d) and (e) CL maps with $\lambda = 430 \pm 5$ nm of bulk and lamella sample, respectively, with pixel sizes of 10 and 25 nm. The orange box in (d) indicates the scan area in (e). The spectra from the same two positions of the bulk and lamella sample are plotted in (f) and (g).

Due to the rich hyperspectral variation across the sample, the hyperspectral maps centered at $\lambda = 430 \pm 5$ nm in bulk and lamella geometries, as seen in Figs. 3(d) and 3(e), provided a unique spatially resolved signature that enabled accurate correlation before and after lamella preparation. The spectra from the same position in the two sample configurations are plotted in Figs. 3(f) and 3(g). This reveals the same trend that the QW emission is quenched and the QD emission is largely preserved. We also observe in the CL map of the lamella in Fig. 3(e) that some of the localized QDs over the scan area have disappeared. This may be a result of the FIB milling away the platinum protective layer at an angle subsequently leaving the sample partially covered with platinum and partially milling into the InGaN layer.

The optical quenching observed, and thus the decrease in the quantum yield, is intrinsically linked to the recombination rates of both radiative and non-radiative transitions in the material.[32] Moving from steady state to TR-CL experiments enables the study of excitation and recombination dynamics of carriers in a system.[33,34] To measure TR-CL in our SEM, the electron beam was blanked using an

electrostatic beam blanker,[35] and the collected luminescence was directed toward a time-correlated single photon counting (TCSPC) module that builds an arrival time histogram.

The measurements on the bulk sample are shown in Fig. 4(a), where plots i and ii are the TR-CL maps filtered for QD and QW emission, respectively. The pulsed measurements have a coarser spatial resolution because of increased astigmatism from adjusting the gun column parameters to align the crossover position between the blanking plates.[35] However, the same trends we observed in Fig. 1(c) are present—the maps filtered for the two bands are complementary, with the QD emission mostly occupying the perimeter of the scan and the QW emission localized to the center of the scan window. Figure 4(aiii) shows the decay trace associated with the same sample position for both maps. The decay trace from the QDs can be fitted with a single-exponential decay, convolved with a Gaussian to account for the instrument response function (IRF), which is limited by the response of the avalanche photodiodes and the electron pulse width. From our fits we extract that the bulk QD lifetime is 433 ± 1 ps. The decay of the QW emission, on the other hand, is fit with a biexponential equation, with a rise time, τ_{rise}, and two decay components of recombination rates τ_1 and τ_2,

$$I_{\mathrm{QW,\,bulk}}(t) = A_1 * \left(1 - e^{\frac{-t}{\tau_{rise}}}\right) * e^{\frac{-t}{\tau_1}} + A_2 * \left(1 - e^{\frac{-t}{\tau_{rise}}}\right) * e^{\frac{-t}{\tau_2}}. \quad (1)$$

The results of the fits give $\tau_{rise} = 125 \pm 3$ ps, $\tau_1 = 1.864 \pm 0.031$ ns, and $\tau_2 = 7.495 \pm 0.136$ ns. The QW decay additionally has a high background because of the contribution from the yellow band emission tail of GaN, which has a lifetime in the μs range.[36] As a repetition rate of 10 MHz was used to maintain a high CL signal, the yellow band does not fully relax into its ground state. Most studies fit InGaN QW recombination with a biexponential function with a fast and slow decay component, associated with the recombination of free or weakly localized excitons and strongly localized excitons, respectively.[37–39] While these studies were performed at low temperatures where emission is excitonic, at room temperature recombination is dominated by free carriers. Similarly, the rise time of the QW peak has been previously attributed to carrier transport from weakly to strongly localized states.[40,41] Our time-resolved measurements performed at liquid nitrogen temperatures (S4) also show that the lifetimes of both the fast and slow decay components increase, and by extension the rise time. In contrast, the QD emission exhibits no measurable rise time, consistent with carriers being localized within strongly confined potential minima. However, we note that due to the convolution with the IRF, a small rise time component cannot be precisely resolved. The single-exponential QD emission implies a more uniform localization of carriers, with their smaller size increasing the e–h overlap and possibly leading to a reduction in the radiative lifetime.[42,43] Conversely, the increased influence of the GaN surface in QDs, which has been demonstrated as a source of non-radiative defects, may also play a role in increasing the recombination rate of the QD.[44]

The time-resolved measurements following lamella preparation, filtered for QD and QW emission, are plotted in Figs. 4(bi) and 4(bii), with corresponding decay traces plotted in Fig. 4(biii). The QD emission can still be fitted with a single-exponential decay and shows a reduction of lifetime to 320 ± 20 ps. The rise time of the QW emission was reduced below the time resolution of the experiment and therefore could be fitted with a standard biexponential, resulting in fit parameters of about $\tau_1 = 111 \pm 7$ ps and $\tau_2 = 550 \pm 113$ ps. The decrease in lifetimes of both emission components is indicative of the introduction of non-radiative defects that quench and decrease the decay time of excited-state populations. FIB is known to introduce point defects, such as vacancies and interstitials, that are believed to generate deep-level trap states that promote non-radiative Shockley–Read–Hall recombination and quench luminescence.[45] The more pronounced quenching of QW emission, compared to QDs, can be attributed to different carrier confinement characteristics. QWs allow for lateral carrier diffusion, enabling carriers to migrate into nearby FIB-induced non-radiative recombination centers, and QDs exhibit three-dimensional confinement, localizing carriers and shielding them from defects. Despite the overall reduction in lifetime, these values still vary along the sample, as shown in the fitted lifetime maps in S5. These variations are not strongly correlated with intensity, particularly for the fast QW decay, that could suggest that carrier recombination through

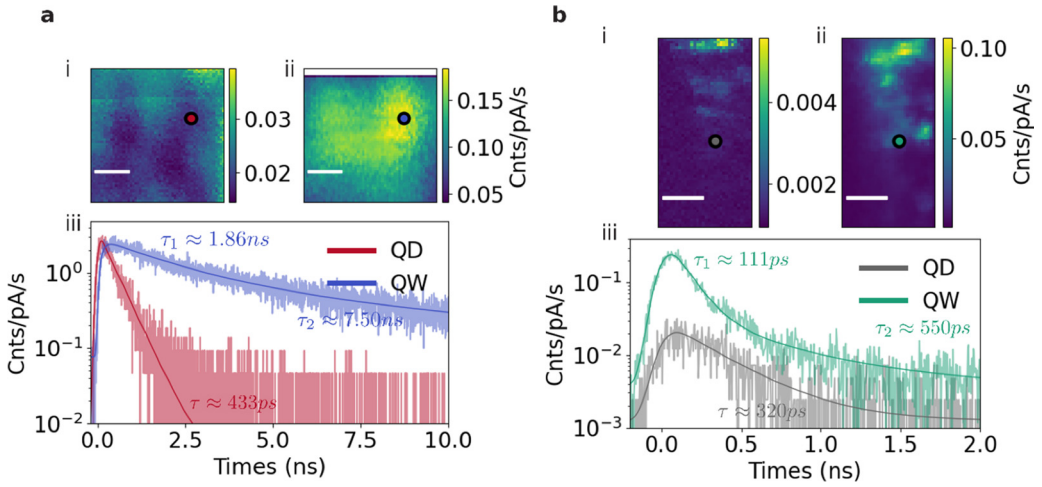

FIG. 4. Comparing SEM-CL lifetime measurements of sample in (a) bulk and (b) lamella configuration. Intensity maps of 35 nm pixel size filtered for (i) $\lambda = 450 \pm 20$ nm and (ii) $\lambda = 550 \pm 20$ nm emission, with markers representing positions of decay transients plotted in (iii). The scale bars are 500 nm in all images.

non-radiative defects is shortening lifetime even in regions of high emission intensity.

We repeated our measurements on a cross-sectional lamella and tested if the optical properties are further influenced by the GaN/vacuum interface. By directly comparing the same area before and after lamella preparation (S6), we observed consistent results, with both plan- and cross-view configurations demonstrating the similar suppression of the QW component in hyperspectral CL measurements as well as comparable reduction in lifetime of both QD and QW emission components. However, nominally identical FIB parameters do not always exhibit identical changes in optical properties. Another plan-view lamella prepared from the same InGaN heterostructure under the same target environmental conditions, milling angles, and beam settings showed less quenching of the QW emission and different average recombination lifetimes (S7). This discrepancy highlights the sensitivity to subtle, uncontrollable factors, primarily the precision of sample and milling box alignment by FIB operators,[46] and drift caused by beam and vacuum instability and sample charging effects. Interestingly, time-resolved photoluminescence (TR-PL) measurements on the lamella also filtered for QD and QW emission (S8) show a shorter lifetime than measured using CL. This discrepancy likely arises from differences in the excitation profile and carrier densities; the electron beam excites carriers throughout the GaN bulk that diffuse into the InGaN,[47] whereas TR-PL at $\lambda = 397$ nm excites carriers directly within the InGaN.

In conclusion, this study demonstrates a nanoscale correlation of spectral and time-resolved luminescence properties of an InGaN/GaN quantum well sample in both its bulk configuration and as FIB lamellae. We observed that the spectra from the bulk sample demonstrate two emission components, arising from the QWs and QD structures formed by the etching of the InGaN layer during fabrication. Our measurements demonstrated that while the QD emission is largely preserved, the QW emission is strongly quenched by lamella preparation, with a significant reduction in lifetime. This effect is attributed to non-radiative defects introduced by the ion beam, which predominantly affect the QW emission due to the weak localization of carriers. Our further analysis of other lamellae prepared under nominally identical conditions of the same bulk sample reveals variable levels of optical quenching, emphasizing the irreproducibility of the artifacts introduced by the FIB. Future work should be wary of optically characterizing materials prepared as lamellae without comparison to their bulk properties.

See the supplementary material for additional details on experimental methods, strain state mapping, Monte Carlo simulations (CASINO), time-resolved and hyperspectral TEM-CL mapping at room temperature, time-resolved SEM-CL measurements at 80 K, correlative SEM-CL measurements on a cross-sectional lamella, SEM-CL measurements on another plan-view lamella, and time-resolved photoluminescence data.

This work is part of the research program of the Dutch Research Council (NWO). This project has received funding from the European Research Council (ERC) under the European Union's Horizon 2020 research and innovation program, Grant Agreement No. 101019932 [Quantum Electron Wavepacket Spectroscopy (QEWS)]. S.M. acknowledges support through the EUR Grant NanoX No. ANR-17-EURE-0009 in the framework of the "Programme des Investissements d'Avenir" and Grant Agreement No. ANR-23-CE09-0018 LUTEM.

AUTHOR DECLARATIONS

Conflict of Interest

Albert Polman is co-founder and co-owner of Delmic BV, a cathodoluminescence system production company like the one that was used in this work.

Author Contributions

Nika van Nielen: Formal analysis (equal); Investigation (equal); Visualization (equal); Writing – original draft (equal). **Luiz H. G. Tizei:** Investigation (equal); Writing – review & editing (supporting). **Delphine Lagarde:** Investigation (supporting); Visualization (supporting); Writing – review & editing (supporting). **Cleo Santini:** Investigation (supporting); Writing – review & editing (supporting). **Florian Castioni:** Investigation (supporting); Writing – review & editing (supporting). **Robin Cours:** Resources (equal); Writing – review & editing (supporting). **Andrea Balocchi:** Supervision (supporting); Writing – review & editing (supporting). **Teresa Hungria:** Investigation (supporting); Writing – review & editing (supporting). **Andrew F. Tsatsulnikov:** Resources (equal); Writing – review & editing (supporting). **Alexei V. Sakharov:** Resources (equal); Writing – review & editing (supporting). **Andrew E. Nikolaev:** Resources (equal); Writing – review & editing (supporting). **Nikolay Cherkashin:** Formal analysis (supporting); Investigation (supporting); Writing – review & editing (supporting). **Albert Polman:** Funding acquisition (equal); Supervision (equal); Writing – review & editing (equal). **Sophie Meuret:** Conceptualization (equal); Formal analysis (equal); Funding acquisition (equal); Project administration (equal); Supervision (equal); Writing – review & editing (equal).

DATA AVAILABILITY

The data that support the findings of this study are available from the corresponding author upon reasonable request.

REFERENCES

[1]K. Thonke, I. Tischer, M. Hocker *et al.*, "Nanoscale characterisation of semiconductors by cathodoluminescence," IOP Conf. Ser.: Mater. Sci. Eng. **55**, 012018 (2014).
[2]P. R. Edwards and R. W. Martin, "Cathodoluminescence nano-characterization of semiconductors," Semicond. Sci. Technol. **26**, 064005 (2011).
[3]K. Loeto, "Uncovering the carrier dynamics of AlInGaN semiconductors using time-resolved cathodoluminescence," Mater. Sci. Technol. **38**, 780–793 (2022).
[4]T. J. O'Hanlon, F. C. P. Massabuau, A. Bao *et al.*, "Directly correlated microscopy of trench defects in InGaN quantum wells," Ultramicroscopy **231**, 113255 (2021).
[5]I. Dimkou, E. Di Russo, P. Dalapati *et al.*, "InGaN quantum dots studied by correlative microscopy techniques for enhanced light-emitting diodes," ACS Appl. Nano Mater. **3**, 10133–10143 (2020).
[6]R. M. Kemper, P. Veit, C. Mietze *et al.*, "STEM-CL investigations on the influence of stacking faults on the optical emission of cubic GaN epilayers and cubic GaN/AlN multi-quantum wells," Phys. Status Solidi C **12**, 469–472 (2015).
[7]F. Bertram, G. Schmidt, J. Kernchen *et al.*, "Direct imaging of the carrier capture into individual InP quantum dots of a semiconductor disk laser membrane," ACS Nano **16**, 4619–4628 (2022).

[8]B. Ding, M. Frentrup, S. M. Fairclough *et al.*, "Multimicroscopy of cross-section zincblende GaN LED heterostructure," J. Appl. Phys. **130**, 115705 (2021).
[9]R. Changizi, S. Zaefferer, L. Abdellaoui *et al.*, "Effects of defect density on optical properties using correlative cathodoluminescence and transmission electron microscopy measurements on identical $PrNbO_4$ particles," ACS Appl. Electron. Mater. **4**, 2095–2100 (2022).
[10]K. Keevend, T. Coenen, and I. K. Herrmann, "Correlative cathodoluminescence electron microscopy bioimaging: Towards single protein labelling with ultrastructural context," Nanoscale **12**, 15588–15603 (2020).
[11]M. I. Mitrofanov, G. V. Voznyuk, S. N. Rodin *et al.*, "Calculation of the Ga^+ FIB ion dose distribution by SEM image," Semiconductors **54**, 1682–1684 (2020).
[12]T. Sato, K. Nakano, H. Matsumoto *et al.*, "High quality lamella preparation of gallium nitride compound semiconductor using Triple Beam^{TM} system," J. Phys.: Conf. Ser. **902**, 012019 (2017).
[13]M. Schaffer, B. Schaffer, and Q. Ramasse, "Sample preparation for atomic-resolution STEM at low voltages by FIB," Ultramicroscopy **114**, 62–71 (2012).
[14]S. Bals, W. Tirry, R. Geurts *et al.*, "High-quality sample preparation by low kV FIB thinning for analytical TEM measurements," Microsc. Microanal. **13**, 80–86 (2007).
[15]A. Wolff, *Focused Ion Beams: An Overview of the Technology and Its Capabilities* (Wiley Analytical Science, 2020).
[16]A. V. Sakharov, S. O. Usov, S. N. Rodin *et al.*, "Effect of annealing on luminescence of InGaN/GaN structures etched by a focused ion beam," Semiconductors **53**, 2121–2124 (2019).
[17]K. Loeto, S. M. Fairclough, I. Griffiths *et al.*, "Influence of Xe^+ and Ga^+ milling species on the cathodoluminescence of wurtzite and zincblende GaN," J. Appl. Phys. **136**, 045702 (2024).
[18]F. U. Kosasih, G. Divitini, J. F. Orri *et al.*, "Optical emission from focused ion beam milled halide perovskite device cross-sections," Microsc. Res. Tech. **85**, 2351–2355 (2022).
[19]A. F. F. Tsatsulnikov, W. V. V. Lundin, A. V. V. Sakharov *et al.*, "Formation of three-dimensional islands in the active region of InGaN based light emitting diodes using a growth interruption approach," Sci. Adv. Mater. **7**, 1629–1635 (2015).
[20]N. Cherkashin, A. Louiset, A. Chmielewski *et al.*, "Quantitative mapping of strain and displacement fields over HR-TEM and HR-STEM images of crystals with reference to a virtual lattice," Ultramicroscopy **253**, 113778 (2023).
[21]I. Olaniyan, I. Tikhonov, V. V. Hevelke *et al.*, "Switchable topological polar states in epitaxial $BaTiO_3$ nanoislands on silicon," Nat. Commun. **15**, 10047 (2024).
[22]N. A. Bert, V. V. Chaldyshev, N. A. Cherkashin *et al.*, "Metallic AsSb nanoinclusions strongly enriched by Sb in AlGaAsSb metamaterial," J. Appl. Phys. **125**, 145106 (2019).
[23]S. N. Mohammad and H. Morkoc, "Progress and progress of group-III nitride semiconductors," Prog. Quantum Electron. **20**, 361–525 (1996).
[24]G. Callsen, R. Butté, and N. Grandjean, "Probing alloy formation using different excitonic species: The particular case of InGaN," Phys. Rev. X **9**, 031030 (2019).
[25]C. Adelmann, J. Simon, G. Feuillet *et al.*, "Self-assembled InGaN quantum dots grown by molecular-beam epitaxy," Appl. Phys. Lett. **76**, 1570–1572 (2000).
[26]L. K. Lee, L. Zhang, H. Deng *et al.*, "Room-temperature quantum-dot-like luminescence from site-controlled InGaN quantum disks," Appl. Phys. Lett. **99**, 263105 (2011).
[27]D. Barettin, A. V. Sakharov, A. F. Tsatsulnikov *et al.*, "Impact of local composition on the emission spectra of InGaN quantum-dot LEDs," Nanomaterials **13**, 1367 (2023).
[28]H.-M. Kim and T.-W. Kang, "Cathodoluminescence characteristics of InGaN/GaN quantum wells grown by MOCVD," Mater. Lett. **48**, 263–268 (2001).
[29]D. Drouin, A. R. Couture, D. Joly *et al.*, "CASINO V2.42—A fast and easy-to-use modeling tool for scanning electron microscopy and microanalysis users," Scanning **29**, 92–101 (2007).
[30]L. F. Zagonel, L. H. G. Tizei, G. Z. Vitiello *et al.*, "Nanometer-scale monitoring of quantum-confined Stark effect and emission efficiency droop in multiple GaN/AlN quantum disks in nanowires," Phys. Rev. B **93**, 205410 (2016).
[31]L. F. Zagonel, S. Mazzucco, M. Tence *et al.*, "Nanometer scale spectral imaging of quantum emitters in nanowires and its correlation to their atomically resolved structure," Nano Lett. **11**, 568–573 (2011).
[32]I. Pelant and J. Valenta, *Luminescence Spectroscopy of Semiconductors* (Oxford University Press, Oxford, 2012).
[33]J. R. Lakowicz, *Principles of Fluorescence Spectroscopy* (Springer, Boston, MA, 2019).
[34]S. Meuret, T. Coenen, S. Y. Woo *et al.*, "Nanoscale relative emission efficiency mapping using cathodoluminescence $g^{(2)}$ imaging," Nano Lett. **18**, 2288–2293 (2018).
[35]S. Meuret, M. Solà Garcia, T. Coenen *et al.*, "Complementary cathodoluminescence lifetime imaging configurations in a scanning electron microscope," Ultramicroscopy **197**, 28–38 (2019).
[36]M. A. Reshchikov, "On the origin of the yellow luminescence band in GaN," Phys. Status Solidi B **260**, 2200488 (2023).
[37]K. Loeto, G. Kusch, O. Brandt *et al.*, "Investigating the exciton dynamics in InGaN/GaN core-shell nanorods using time-resolved cathodoluminescence," Nanotechnology **36**, 025703 (2025).
[38]G. E. Weng, W. R. Zhao, S. Q. Chen *et al.*, "Strong localization effect and carrier relaxation dynamics in self-assembled InGaN quantum dots emitting in the green," Nanoscale Res. Lett. **10**, 31 (2015).
[39]P. Dawson, S. Schulz, R. A. Oliver *et al.*, "The nature of carrier localisation in polar and nonpolar InGaN/GaN quantum wells," J. Appl. Phys. **119**, 181505 (2016).
[40]Y. Robin, E. A. Evropeitsev, T. V. Shubina *et al.*, "Localization and transient emission properties in InGaN/GaN quantum wells of different polarities within core-shell nanorods," Nanoscale **11**, 193–199 (2019).
[41]S. W. Feng, Y. C. Cheng, Y. Y. Chung *et al.*, "Impact of localized states on the recombination dynamics in InGaN/GaN quantum well structures," J. Appl. Phys. **92**, 4441–4448 (2002).
[42]Y. R. Wu, Y. Y. Lin, H. H. Huang *et al.*, "Electronic and optical properties of InGaN quantum dot based light emitters for solid state lighting," J. Appl. Phys. **105**, 013117 (2009).
[43]A. David, N. G. Young, C. Lund *et al.*, "Review—The physics of recombinations in III-nitride emitters," ECS J. Solid State Sci. Technol. **9**, 016021 (2020).
[44]C. Haller, J. Carlin, G. Jacopin *et al.*, "GaN surface as the source of non-radiative defects in InGaN/GaN quantum wells," Appl. Phys. Lett. **113**, 111106 (2018).
[45]I. H. Lee, A. Y. Polyakov, N. B. Smirnov *et al.*, "Point defects controlling non-radiative recombination in GaN blue light emitting diodes: Insights from radiation damage experiments," J. Appl. Phys. **122**, 115704 (2017).
[46]H. Tsurusawa, N. Nakanishi, K. Kawano *et al.*, "Robotic fabrication of high-quality lamellae for aberration-corrected transmission electron microscopy," Sci. Rep. **11**, 21599 (2021).
[47]S. M. Olaizola, W. H. Fan, S. A. Hashemizadeh *et al.*, "Time-resolved photoluminescence studies of carrier diffusion in GaN," Appl. Phys. Lett. **89**, 072107 (2006).